Journal of Biomedical Optics

SPIEDigitalLibrary.org/jbo

Wide-field fast-scanning photoacoustic microscopy based on a water-immersible MEMS scanning mirror

Junjie Yao
Chih-Hsien Huang
Lidai Wang
Joon-Mo Yang
Liang Gao
Konstantin I. Maslov
Jun Zou
Lihong V. Wang

SPIE

Wide-field fast-scanning photoacoustic microscopy based on a water-immersible MEMS scanning mirror

Junjie Yao,[a*] Chih-Hsien Huang,[b*] Lidai Wang,[a] Joon-Mo Yang,[a] Liang Gao,[a] Konstantin I. Maslov,[a] Jun Zou,[b] and Lihong V. Wang[a]

[a]Washington University in St. Louis, Optical Imaging Laboratory, Department of Biomedical Engineering, St. Louis, Missouri 63130
[b]Texas A&M University, Department of Electrical and Computer Engineering, College Station, Texas 77843

Abstract. By offering images with high spatial resolution and unique optical absorption contrast, optical-resolution photoacoustic microscopy (OR-PAM) has gained increasing attention in biomedical research. Recent developments in OR-PAM have improved its imaging speed, but have to sacrifice either the detection sensitivity or field of view or both. We have developed a wide-field fast-scanning OR-PAM by using a water-immersible microelectromechanical systems (MEMS) scanning mirror (MEMS-OR-PAM). In MEMS-OR-PAM, the optical and acoustic beams are confocally configured and simultaneously steered, which ensures the uniform detection sensitivity. A B-scan imaging speed as high as 400 Hz can be achieved over a 3 mm scanning range. Using the system, we imaged the flow dynamics of both red blood cells and carbon particles in a mouse ear *in vivo*. Presented results show that MEMS-OR-PAM could be a powerful tool for studying highly dynamic and time-sensitive biological phenomena. [DOI: 10.1117/1.JBO.17.8.080505]

Keywords: optical-resolution photoacoustic microscopy; fast scanning; MEMS scanning mirror; blood flow dynamics; confocality; confocal sensitivity.

Paper 12347L received Jun. 1, 2012; revised manuscript received Jul. 19, 2012; accepted for publication Jul. 24, 2012; published online Aug. 14, 2012.

As a major implementation of photoacoustic tomography, optical-resolution photoacoustic microscopy (OR-PAM) has been proven capable of anatomical, chemical, functional, and metabolic imaging.[1–8] OR-PAM provides a capillary-level spatial resolution by tightly focusing the laser beam at depths within the optical diffusion limit (~1 mm in the skin).[1,2] The main feature of OR-PAM is the confocal configuration of the optical and acoustic beams, which maximizes the detection sensitivity. Recently, the spatial resolution of OR-PAM has been improved to 220 nm by using a water-immersion objective with 1.23 numerical aperture (NA).[9] A double-illumination OR-PAM has been developed to extend the imaging depth to 2 mm by illuminating both the top and bottom surfaces of a thin sample.[10] As all living biological systems are dynamic, it is also important to develop fast-scanning OR-PAM systems.

Several scanning mechanisms have been reported to push the imaging speed of OR-PAM. The first type is to optically scan the laser beam within the focal spot of the ultrasonic transducer.[11,12] This mechanism, however, suffers from a limited scanning range of ~100 μm and inhomogeneous detection sensitivity within the field of view (FOV).[11,12] The second method is to optically scan the laser beam within the detection area of an unfocused ultrasonic transducer.[11,13] This method increases the scanning range to a few millimeters while reducing the overall detection sensitivity by more than 40 dB. The third form is to mechanically scan by mounting the whole imaging head on a voice-coil scanner.[14] This design can maintain the confocal alignment and increase the scanning range to a few millimeters, but over which the scanning speed can reach only ~40 Hz, limited by the mass of the imaging head.

Here, we present a wide-field fast-scanning OR-PAM by using a lab-made water-immersible microelectromechanical systems (MEMS) scanning mirror (MEMS-OR-PAM). A cross-sectional (B-scan) imaging rate of 400 Hz over a 3 mm range has been achieved. By scanning both the excitation laser beam and resultant acoustic beam, MEMS-OR-PAM maintains confocal alignment and high detection sensitivity over a large FOV.

Figure 1 is a schematic of the MEMS-OR-PAM. The light source is an $Nd:YVO_4$ laser (AOT-YVO-100Q, AOT Inc.,) that generates 2 ns pulses at 532 nm with a repetition rate of 100 kHz. The laser beam is focused by a condenser lens (LA1131, Thorlabs) then spatially filtered by a 50 μm diameter pinhole (P50C, Thorlabs). The filtered beam is focused by an optical objective lens (AC127-050-A, Thorlabs. NA: 0.1 in air). A beam combiner composed of an aluminum-coated prism (NT32-331, Edmund) and an uncoated prism (NT32-330, Edmund) provides acoustic-optical coaxial alignment. The thin aluminum coating provides optical reflection but acoustic transmission. The focused laser beam is directed toward the sample surface by the aluminum coating of the combiner and a MEMS scanning mirror plate. An optical correction lens attached to the top surface of the combiner corrects the aberration due to the prism. The resultant photoacoustic waves are reflected by the MEMS scanning mirror and detected by an ultrasonic transducer (V214-BB-RM, Olympus-NDT), which has a central frequency of 50 MHz and a −6 dB bandwidth of 100%. An acoustic lens with a NA of 0.25 (NT45-010, Edmund) is attached to the right surface of the combiner and provides an acoustic focal spot size of ~80 μm in water. The acoustic NA of this system is chosen to be ~50% less than that of previously reported OR-PAM systems because fitting the MEMS scanning mirror requires a longer working distance. The whole imaging head is submerged in a water tank for ultrasound coupling. Volumetric imaging is provided by fast angular scanning of the MEMS scanning mirror along the x-axis and step motor scanning of the sample along the y-axis.

The 9×9 mm^2 MEMS mirror plate (thickness: 0.5 mm) is made of silicon with an 80-nm-thick gold coating, thus provides a good reflection of both the optical and acoustic beams. The mirror plate is supported by two 1×0.9 mm^2 hinges made

*These authors contributed equally to this work.

Address all correspondence to: Lihong V. Wang, Washington University in St. Louis, Optical Imaging Laboratory, Department of Biomedical Engineering, St. Louis, Missouri 63130. E-mail: lhwang@wustl.edu.

0091-3286/2012/$25.00 © 2012 SPIE

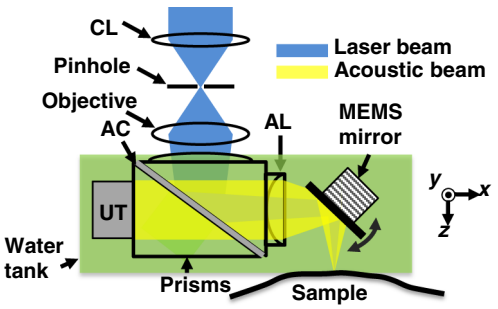

Fig. 1 Schematic of MEMS-OR-PAM. CL, condenser lens; AC, aluminum coating; AL, acoustic lens; UT, ultrasonic transducer.

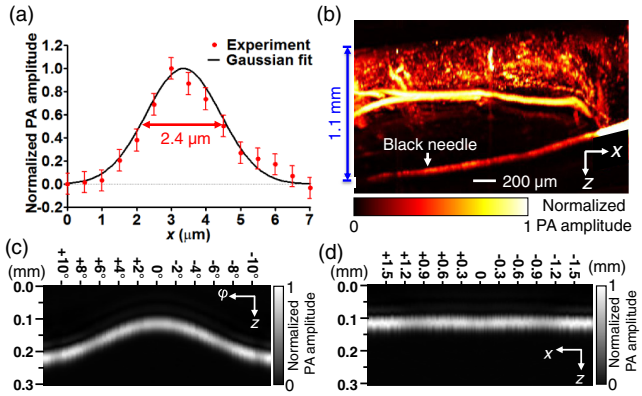

Fig. 2 Characteristics of MEMS-OR-PAM. (a) Line spread function used to measure the lateral resolution of the system (red circles, the averaged pixel values; black line, the Gaussian fit). (b) MEMS-OR-PAM image of a black needle inserted obliquely into the leg of a living mouse. A 1.1 mm *in vivo* imaging depth was achieved with time-gain compensation. (c) Raw B-scan image of a piece of flat black-tape in polar coordinates. The angular scanning of the MEMS mirror introduced the curvature of the imaged target surface. φ, scanning angle of the MEMS mirror. (d) B-scan image in Cartesian coordinates converted based on the scanning geometry and 2D linear interpolation.

of high-strength flexible polymer materials, which can resist surface tension forces in liquids. To actuate the mirror, high efficient electromagnetic force is generated by a compact inductor coil (inductance: 33 mH) and a pair of high-strength rare-earth permanent magnets (diameter: 3.1 mm) on the back of the mirror plate. A sinusoidal current applied to the inductor coil generates a magnetic field with alternating polarity and strength, which drives the mirror plate to oscillate around the hinges. By controlling the frequency and amplitude of the driving voltage, the scanning speed and range can be adjusted appropriately.

To measure the lateral resolution of the MEMS-OR-PAM system, the edge of a sharp blade was imaged in water, with a step size of 0.5 μm and a scanning range of 100 μm along the x-axis. From the edge spread function, the full width at half maximum of the line spread function is estimated to be 2.4 μm, which is close to the theoretical, diffraction-limited focal spot size of the laser beam (2.1 μm) [Fig. 2(a)]. The optical focal zone is about 100 μm, in which the lateral resolution is within 10 μm. The axial resolution was estimated to be ~26 μm based on the transducer bandwidth and the speed of sound in tissue. Both the lateral and the axial resolutions decrease with imaging depth due to increasing optical scattering and frequency-dependent acoustic attenuation in tissue, respectively. The maximum penetration depth of the MEMS-OR-PAM was experimentally quantified by obliquely inserting a 250 μm diameter black needle into the leg of an anesthetized nude mouse. As shown in Fig. 2(b), after time-gain compensation for the optical and acoustic attenuation, the system can clearly image the needle down to 1.1 mm beneath the skin surface, which is comparable to other OR-PAM systems.[14,15] Different from the linear scanning of traditional OR-PAM systems,[3,14,15] the angular scanning of MEMS-OR-PAM results in a curved focal plane with a radius of 7 mm. The maximum in-focus scanning range is ~3.0 mm along the x-axis. Since raw B-scan images are in the polar coordinates [Fig. 2(c)], we converted the data to Cartesian coordinates considering the scanning geometry and applying a 2D linear interpolation [Fig. 2(d)]. For a uniform black-tape target, the averaged PA signal amplitude varies less than 5% along the x-axis [Fig. 2(d)]. The result demonstrates that MEMS-OR-PAM maintains uniform detection sensitivity along the scanning direction, superior to other fast scanning methods where the confocality is compromised.

Red blood cell (RBC) flow in a nude mouse ear was imaged *in vivo* by MEMS-OR-PAM to demonstrate its high-speed imaging capability. All experimental animal procedures were carried out in conformity with the laboratory animal protocol approved by the Animal Studies Committee at Washington University in St. Louis. As shown in Fig. 3, a 2×5 mm^2 area of the mouse ear was repeatedly scanned with a volumetric imaging speed of 0.8 Hz (a 2D B-scan rate of 400 Hz), which is about 400 times faster than the second-generation OR-PAM system and 20 times faster than the most recent voice-coil based OR-PAM scanner for the same scanning range.[14,15] The laser pulse energy on the skin surface was measured to be 100 nJ. The lateral step size was 12 μm along the x-axis and 10 μm along the y-axis, limited by the laser repetition rate of 100 kHz. The step motor scanning speed was 4 mm/s. The total pixel number for each image was 125,000. Since 532 nm is close to the isosbestic wavelength, the PA signal amplitude reflects the total hemoglobin concentration regardless of the oxygenation of hemoglobin. The spatial resolution is sufficient for resolving the capillary beds (Fig. 3), and the imaging speed enables the mapping of the RBC movements in small vessels (Video 1). Theoretically, we should be able to capture RBCs flowing at 1.6 mm/s along the x-axis and 4 mm/s along the y-axis. In a nude mouse ear, such a speed range should cover the veins with diameters less than 130 μm and arteries with diameters less than 30 μm.[16] The average signal to noise ratio (SNR) is 36.5 dB, which is about 6 dB less than that of the second-generation OR-PAM system, due to the smaller NA of the employed acoustic lens.[15] Nevertheless, this SNR is adequate for single RBC imaging.[14,15]

In addition to the RBC flow imaging based on endogenous contrast, intravascular transport of an exogenous contrast agent was also explored using the system. First, we imaged a 0.6×2 mm^2 area of a nude mouse ear as a control with laser pulse energy of 100 nJ [Fig. 4(a)]. Then, we injected carbon particles with ~6 μm diameters (2.5% w/v, carbon glassy spherical powder, Sigma-Aldrich) into the blood stream of the nude mouse via its tail vein. A 0.3×1 mm^2 area, which contained a 40 μm diameter vein, was chosen as the region of interest (ROI) for dynamic imaging. The lateral step size was 2 μm along the x-axis and 10 μm along the y-axis. The step motor scanning speed was 4 mm/s. The ROI was repeatedly imaged with a volumetric frame rate of 4 Hz. The total pixel number for each image was 25,000. Lower pulse energy of 10 nJ was

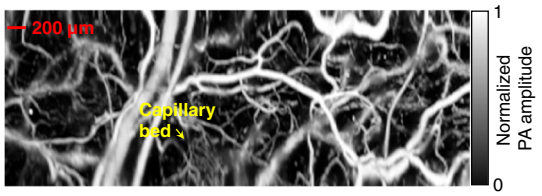

Fig. 3 MEMS-OR-PAM of blood flow dynamics of the vasculature in a mouse ear. Capillaries were clearly resolved, and the flow dynamics over a 2×5 mm^2 area were imaged with a 0.8 Hz volumetric frame rate and 400 Hz B-scan rate. (Video 1, MPEG, 8.8 MB) [URL: http://dx.doi.org/10.1117/1.JBO.17.8.080505.1.]

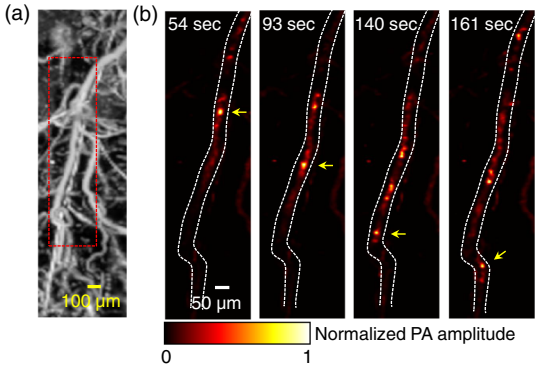

Fig. 4 MEMS-OR-PAM of flow dynamics of carbon particles. (a) MEMS-OR-PAM image of a mouse ear with a pulse energy of 100 nJ, where the blood vessels were imaged. (b) After the injection of carbon particles via the tail vein, a smaller region indicated by the dashed box in (a) was monitored with a 4 Hz volumetric frame rate. The pulse energy was reduced to 10 nJ to image only the particles. The dashed lines are the boundaries of the vessel containing the flowing particles. A representative particle is indicated by the arrows. (Video 2, MPEG, 8.8 MB) [URL: http://dx.doi.org/10.1117/1.JBO.17.8.080505.2.]

used to image only the particles, which are much more absorbing than hemoglobin. As shown in Fig. 4(b) and Video 2, the average flow speed of the particles in the vein was much slower than the RBC flow.[5] This is likely due to the larger mass density of the particles (1.46 g/cm^3).

In summary, we have developed MEMS-OR-PAM that can dramatically improve the imaging speed while maintaining the confocal alignment of the optical and acoustic beams over a wide FOV. Conserving the high spatial resolution and imaging sensitivity of traditional OR-PAM systems, we achieved a B-scan imaging speed of 400 Hz over a 3 mm scanning range. The scanning range, lateral resolution, and imaging speed can be traded for each other. A laser system with higher repetition rate or an intensity-modulated continuous wave laser can further improve the imaging speed while maintaining the high resolution and wide scanning range. By employing a dual-wavelength laser source, MEMS-OR-PAM is intrinsically capable of label-free measurements of oxygen saturation and oxygen metabolism.[4]

Acknowledgments

The authors appreciate Prof. James Ballard's close reading of the manuscript. This work was sponsored by NIH grants R01 EB000712, R01 EB008085, R01 CA134539, U54 CA136398, R01 CA157277, and R01 CA159959 (for L. V. Wang), and NSF grant CMMI-1131758 (for J. Zou). L. V. Wang has a financial interest in Endra, Inc., and Microphotoacoustics, Inc., which, however, did not support this work. K. I. Maslov has a financial interest in Microphotoacoustics, Inc., which did not support this work.

References

1. L. V. Wang, "Multiscale photoacoustic microscopy and computed tomography," *Nat. Photonics* **3**(9), 503–509 (2009).
2. L. H. V. Wang and S. Hu, "Photoacoustic tomography: *in vivo* imaging from organelles to organs," *Science* **335**(6075), 1458–1462 (2012).
3. K. Maslov et al., "Optical-resolution photoacoustic microscopy for *in vivo* imaging of single capillaries," *Opt. Lett.* **33**(9), 929–931 (2008).
4. J. Yao et al., "Label-free oxygen-metabolic photoacoustic microscopy *in vivo*," *J. Biomed. Opt.* **16**(7), 076003 (2011).
5. J. Yao et al., "*In vivo* photoacoustic imaging of transverse blood flow by using Doppler broadening of bandwidth," *Opt. Lett.* **35**(9), 1419–1421 (2010).
6. M. R. Chatni et al., "Functional photoacoustic microscopy of pH," *J. Biomed. Opt.* **16**(10), 100503 (2011).
7. A. Krumholz et al., "Photoacoustic microscopy of tyrosinase reporter gene *in vivo*," *J. Biomed. Opt.* **16**(8), 080503 (2011).
8. A. Krumholz et al., "Functional photoacoustic microscopy of diabetic vasculature," *J. Biomed. Opt.* **17**(6), 060502 (2012).
9. C. Zhang, K. Maslov, and L. V. Wang, "Subwavelength-resolution label-free photoacoustic microscopy of optical absorption *in vivo*," *Opt. Lett.* **35**(19), 3195–3197 (2010).
10. J. Yao et al., "Double-illumination photoacoustic microscopy," *Opt. Lett.* **37**(4), 659–661 (2012).
11. B. Rao et al., "Real-time four-dimensional optical-resolution photoacoustic microscopy with Au nanoparticle-assisted subdiffraction-limit resolution," *Opt. Lett.* **36**(7), 1137–1139 (2011).
12. W. Shi and R. J. Zemp, "Label-free *in vivo* fiber-based optical-resolution photoacoustic microscopy," *Opt. Lett.* **36**(20), 4107–4109 (2011).
13. Z. X. Xie et al., "Laser-scanning optical-resolution photoacoustic microscopy," *Opt. Lett.* **34**(12), 1771–1773 (2009).
14. L. D. Wang et al., "Fast voice-coil scanning optical-resolution photoacoustic microscopy," *Opt. Lett.* **36**(2), 139–141 (2011).
15. S. Hu, K. Maslov, and L. V. Wang, "Second-generation optical-resolution photoacoustic microscopy with improved sensitivity and speed," *Opt. Lett.* **36**(7), 1134–1136 (2011).
16. J. H. Barker et al., "The hairless mouse ear for *in vivo* studies of skin microcirculation," *Plast. Reconstr. Surg.* **83**(6), 948–959 (1989).